Magnetization reversal due to vortex nucleation, displacement, and annihilation in submicron ferromagnetic dot arrays

K. Yu. Guslienko
School of Physics, Korea Institute for Advanced Study, Seoul 130-012, Korea

V. Novosad,* Y. Otani, H. Shima, and K. Fukamichi
Department of Materials Science, Tohoku University, Aoba-yama 02, Sendai 980-8579, Japan
(Received 7 August 2001; published 14 December 2001)

Magnetization processes are analytically described for the arrays of soft ferromagnetic polycrystalline circular dots with submicron dimensions, wherein the magnetization reversal accompanied by nucleation, displacement, and annihilation of magnetic vortices. Magnetostatic, exchange, and Zeeman energies are taken into account for the analysis. The magnetic state of each dot in an applied magnetic field is treated as an off-centered rigid vortex structure; i.e., the vortex keeps its spin distribution while being displaced. This rigid vortex model yields analytical expressions for the size-dependent initial susceptibility, the vortex nucleation, and the annihilation fields. The interdot magnetostatic interaction plays an important role in the magnetization reversal for the arrays when the interdot distance is smaller than the disk radius, where the initial susceptibility increases and both the nucleation and annihilation fields decrease. The analytical predictions are compared to the micromagnetic calculations, and limitations of the model are discussed.

DOI: 10.1103/PhysRevB.65.024414 PACS number(s): 75.75.+a, 75.60.Jk, 75.30.Gw

I. INTRODUCTION

Recent interest in magnetic systems with reduced dimensions has been stimulated by the rapid evolution of various microfabrication techniques. In particular, it enables us to fabricate well-defined two-dimensional arrays of submicron ferromagnetic particles (dots). This offers various opportunities to test new concepts of *spintronic* devices, such as magnetic random access memory (MRAM),[1] high-density patterned recording media,[2,3] and ultrasmall magnetic field sensors.[4] Prior to the technological applications mentioned above, it is indispensable to understand well fundamental properties of the individual and interacting magnetic elements with reduced dimensions.

It is generally recognized that theoretical description of the magnetization reversal process in a real ferromagnet is rather complicated, since one should consider all the energy terms composed of exchange, magnetocrystalline anisotropy, and magnetostatic contributions.[5] Therefore, the arrays of identical dots fabricated by the microlithography process are considered as a model system well suited for direct comparison between calculations and experiments. Controlling both dot geometry and crystal microstructure is a challenging and achievable task. For example, in single-crystalline epitaxial dots, the magnetocrystalline anisotropy plays an important role in determining the demagnetization process, and the effective anisotropy is adjusted to the desirable strength. The spin-reorientation transitions caused by interplay between the shape and temperature-dependent magnetocrystalline anisotropies have been observed in epitaxial rectangular Co dots.[6,7] The magnetic behavior of the polycrystalline systems is mainly determined by their geometry and shape due to lack of microscopic crystalline order. This tendency has been demonstrated for arrays of flat polycrystalline dots with circular,[8,9] elliptical,[10,11] rectangular,[8,12] and triangular[13] shapes.

The remanent domain structure of ideal magnetically soft dot is determined by the disk aspect ratio $\beta = L/R$ and the exchange length $R_0 = \sqrt{C/M_s^2}$, where L is the dot thickness, R the disk radius, C the magnetic exchange stiffness constant, and M_s the saturation magnetization. There are three stable magnetic structures for small enough R and L, when the formation of magnetic domains and domain walls is not energetically favored. Two of them in the first approximation can be described as single-domain states with magnetization parallel and perpendicular to the disk basal plane when $\beta < 1.81$ with $L \leqslant R_0$, $R < R_c(L)$, and $\beta > 1.81$ with $R \leqslant R_0$, respectively. The value of $\beta = 1.81$ is the critical aspect ratio for the reorientation transition for a single-domain cylindrical dot.[14] The other is the ''vortex''-type spin distribution when $R > R_c(L)$, the critical radius for the vortex stability. The vortex spin structure was experimentally observed in submicron disks with thickness of about several tens of nanometers. For example, Lorenz electron microcopy was employed to study a field-dependent vortex evolution in permalloy disks.[15] The size dependences of vortex nucleation/annihilation fields have been studied experimentally for circular Permalloy[8,16,17] and ellipsoidal cobalt dots.[10] The magnetic force microscope (MFM) observations of the magnetic vortex states in remanence[18] and under an applied field[19] have been reported. The vortex nucleation in Permalloy particles was reported to cause an incomplete magnetization reversal, which originates the failure in operating MRAM cells.[20] On the other hand, the submicron circular dots and ring-type nanostructures with a high stability of remanent vortex state have been proposed as possible candidates for bistable magnetic memories.[21,22]

To our knowledge, there are neither theoretical and experimental analyses nor micromagnetic data related to the effect of interdot magnetostatic coupling on the demagnetizing process in the dot arrays with nonuniform remanent state

such as the "*vortex*" structures, whereas there are some theoretical works about the magnetization reversal in isolated circular ferromagnetic elements. The realistic curling magnetization distribution in the flat disk was first calculated analytically[14] and then by using a variational approach.[23,24] The vortex stability in remanence and in external magnetic fields was examined respectively in Refs. 24, 25 and 26, respectively.

In this work, we have developed an analytical model to describe how the characteristic properties such as the vortex nucleation H_n and annihilation $H_{\rm an}$ fields and the initial susceptibility $\chi(0)$ depend on the size and interdisk distance. We compare the obtained results with micromagnetic calculations. The paper is composed of five sections as follows. In Sec. II we describe the analytical models for an isolated dot and an array of magnetostatically coupled dots. In Sec. III, we briefly show some issues related to the micromagnetic calculations. The results and applicability of the proposed model are discussed in Sec. IV. Finally, the summary is given in Sec. V.

II. ANALYTICAL MODEL

A. Isolated dot

To begin, we consider the magnetization reversal initiated via the vortex nucleation, the displacement, and the annihilation in an isolated disk. The magnetization curling mode in the flat disk was analytically examined by Aharoni[14] using the cylindrical coordinates, where the z axis the cylinder axis, ρ is the polar radius, φ is the polar angle, and $\mathbf{m}(\mathbf{r})=\mathbf{M}(\mathbf{r})/M_s$ with $m_\rho=0$, $m_\varphi=f(\rho)$, and $m_z=\sqrt{1-m_\varphi^2}$. Usov and Peschany[23,24] have found, from the variational principle, that the replacement $f(\rho)\rightarrow sin\,\vartheta(\rho)$ finally yields the relation $tan\,\vartheta/2=\rho/b$, where b is the radius of the region with $m_z\neq 0$ (vortex core). This solution is valid for a wide range of dot sizes as far as the dot radius R is larger than the critical radius $R_c(L)$. The magnetization unit vector $\mathbf{m}$ rotates out of the dot basal plane when $\rho<b$. The value of b can be evaluated by minimizing the total magnetic energy consisting of the exchange and magnetostatic energies due to surface and volume charges in the dot. Comparison between the numerical and analytical results indicate that the curling type vortex magnetization distribution in a ferromagnetic dot is expressed as

$$m_\rho=0,\quad m_\varphi=\sin\theta(\rho)=\begin{cases}2b\rho/(b^2+\rho^2), & \rho\leqslant b,\\ 1, & \rho>b,\end{cases}$$
$$m_z=\pm\cos\theta(\rho). \tag{1a}$$

Note here that the magnetization distribution does not vary along the z axis. This is correct for disks with thickness L equivalent to the exchange length. It is also clear that the side surface and volume charges are not stored in the distribution given by Eq. (1a). The vortex can be characterized by the out-of-plane (for $\rho<b$) and in-plane (for $\rho>b$) magnetization directions. It is convenient to rewrite the two-dimensional magnetization distribution $\mathbf{m}(x,y)$ given by Eq. (1a) by using dimensionless complex variables $\zeta=(x+iy)/R$ and $w(\zeta,\overline{\zeta})$ (Ref. 26):

$$m_x+im_y=\frac{2w}{1+w\overline{w}},\quad m_z=\frac{1-w\overline{w}}{1+w\overline{w}}, \tag{1b}$$

where the bar over a variable denotes the complex conjugation. The complex function $w(\zeta,\overline{\zeta})$ has the form $w(\zeta,\overline{\zeta})=f(\zeta)$ if $|f(\zeta)|<1$ (within the vortex core) and $w(\zeta,\overline{\zeta})=f(\zeta)/|f(\zeta)|$ if $|f(\zeta)|\geqslant 1$, where $f(\zeta)$ is an appropriate analytical function. In our case $f(\zeta)=(i/c)\zeta$, which is equivalent to Eq. (1a), and $c=b/R$ is the relative core radius.

In the remanent state, the vortex stays at the center of the disk. When the magnetic field is applied, the vortex core is pushed toward the dot perimeter to increase the average magnetization component along the field. We assume that the spin distribution within the vortex is always described by Eq. (1a) while being displaced, i.e., the vortex spin structure remains unchanged. The shifted vortex magnetization distribution is described as $f(\zeta)=(i/c)(\zeta-s)$, where c is the constant, and $s=l/R$ is the relative vortex displacement. The value of $s\cong 1$ requires special consideration where we assume that $|s-1|>c$ with $c\ll 1$. The last assumption is correct for sub-micron-size dots, $R\gg R_0$ ($0.6\leqslant cR/R_0\leqslant 1$ according to Usov and Peschany's calculations[24]).

This simple one-vortex approximation (so-called "rigid" vortex model) is reasonable when (1) the vortex displacement l is much smaller than the disk radius R and (2) the vortex center is outside the dot ($l\gg R$). The two-vortex distribution (one circular vortex is inside the dot and one cross vortex is outside the dot) using the disk conformal mapping $\zeta\rightarrow\zeta'=(\zeta-a)/(1-\overline{a}\zeta)$ was successfully applied to explain the vortex annihilation field by Guslienko and Metlov in Ref. 26. But this mapping cannot explain satisfactorily the vortex initial susceptibility and cannot predict the border of the vortex stability. The function $w(\zeta,\overline{\zeta})$ determines good trial magnetization distribution in a cylindrical dot. Its parameters (s and c in our case) can be found from the total dot magnetic energy minimization.

The total dot magnetic energy consists of the exchange $W_{\rm ex}$, magnetostatic W_m, and Zeeman W_H energies. The magnetocrystalline anisotropy is assumed to be negligible. Here all the energies are normalized to the unit of M_s^2V with the dot volume $V(=\pi R^2L)$. The nonuniform exchange energy $W_{\rm ex}=(C/2)\int d^3\mathbf{r}\Sigma_\alpha(\nabla m_\alpha)^2$, was developed with respect to the vortex center displacement s by taking into account Eq. (1). The exchange energy of the dot in the magnetization curling state of Eq. (1) with the shifted vortex center ($l\leqslant R-b$) is thus given by

$$\frac{W_{\rm ex}}{M_s^2V}=\frac{1}{2\pi}\left(\frac{R_0}{R}\right)^2\int d^2\boldsymbol{\rho}\left[\left(\frac{d\theta}{d\rho}\right)^2+\frac{\sin^2\theta}{\rho^2}\right],$$
$$w_{\rm ex}(s)=w_{\rm ex}(0)+\frac{1}{2}\left(\frac{R_0}{R}\right)^2\ln(1-s^2), \tag{2}$$

where it is assumed that $|s-1|>c$.

The exchange energy $w_{ex}(s)$ decreases with the increase of s. Then expanding Eq. (2) in a series on s yields the exchange energy density

$$w_{ex}(s)=w_{ex}(0)+\left(\frac{R_0}{R}\right)^2\left[-\frac{1}{2}s^2+O(s^4)\right]. \tag{3}$$

For the isolated disk, the Zeeman energy does not depend on the direction of the in-plane external field **H** and is given as

$$W_H(s)=-\int_V d^3\mathbf{r}\,\mathbf{M}(\mathbf{r})\cdot\mathbf{H}$$
$$=-HM_sVs\int_0^\infty dx[J_0(x)J_0(xs)-J_2(x)J_2(xs)]. \tag{4}$$

For the small vortex displacement s, denoting $h=H/M_s$, the Zeeman energy density is thus approximated as

$$w_H(s)=-h(s+O(s^3)). \tag{5}$$

The magnetostatic energy in the model is only generated by the surface magnetic charges $\sigma=(\mathbf{M}\cdot\mathbf{n})$ along the dot perimeter. The volume charges are absent (div$\mathbf{m}=0$), the top and bottom surface charges at $z=0$, and L remains unchanged on the vortex displacement. We thus have

$$W_m=\frac{1}{2}\int dS\int dS'\frac{\sigma(\mathbf{r})\sigma(\mathbf{r}')}{|\mathbf{r}-\mathbf{r}'|}, \tag{6}$$

with

$$\sigma(\mathbf{r})=-M_s\frac{s\sin(\varphi)}{\sqrt{1+s^2-2s\cos(\varphi)}},$$

where the integration is taken for the disk side surface. The vortex displacement is assumed parallel to the x axis (s is real). The dot magnetostatic self-energy is given as follows:

$$\frac{W_m(s)}{M_s^2V}=\frac{2}{\pi}s^2\sum_{\mu>0}F_\mu(\beta)I_\mu^2(s), \tag{7}$$

where

$$F_\mu(\beta)=\int_0^\infty\frac{dt}{t}f(\beta t)J_\mu^2(t),$$

$$I_\mu(s)=2\int_0^\pi d\varphi\frac{\sin(\varphi)\sin(\mu\varphi)}{\sqrt{1-2s\cos(\varphi)+s^2}},$$

and $f(x)=1-[1-\exp(-x)]/x$ and $\beta=L/R$.

This expression is valid for all the values of s. For small s, since $I_\mu^2(s)=\pi^2\delta_{\mu,1}+O(s^2)$, the magnetostatic energy density including the disk top and bottom surface is obtained as

$$w_m(s)=w_m(0)+2\pi F_1(\beta)s^2+O(s^4). \tag{8}$$

The function $F_1(\beta)$ is proportional to the average in-plane demagnetizing factor $N_x(\beta)=4\pi\int dt\,t^{-1}f(\beta t)J_1^2(t)$.[14]

Here we distinguish three characteristic field related to the vortex evolution: the vortex nucleation field H_n, the annihilation field H_{an}, and the field H_0 at which the vortex and saturated (single-domain) states have totally equal magnetic energies. As will be explained below, these three fields satisfy the relation, $H_n<H_0<H_{an}$.

The sum of the energies (3), (5), and (8) gives the total magnetic energy density of the off-centered vortex in a dimensionless form:

$$w(s)=w_{ex}(s)+w_m(s)+w_H(s)$$
$$=w(0)+a(\beta,R)s^2-hs+O(s^4), \tag{9}$$

where

$$a(\beta,R)=2\pi F_1(\beta)-\frac{1}{2}\left(\frac{R_0}{R}\right)^2. \tag{10}$$

We assume that $a(\beta,R)>0$, since this condition is necessary for stabilizing the magnetic vortex in a cylindrical dot within the framework of the ''rigid'' vortex model as proposed by Usov and Peschany in Ref. 24 for $H=0$. The dots considered here satisfy the above condition because the vortex structures are observed in the remanent state ($R>R$).

By minimizing the total magnetic energy in Eq. (9) with respect to s, one can obtain the equilibrium displacement s_0 of the vortex center and the dot average magnetization as function of dot sizes L,R and external field H in the form.

$$s_0=\frac{1}{2a(\beta,R)}h\Rightarrow\langle\mathbf{M}\rangle_V=\frac{1}{2a(\beta,R)}\mathbf{H}, \tag{11}$$

where $\chi_{is}=[2a(\beta,R)]^{-1}$ has sense of the in-plane initial magnetic susceptibility of the isolated disk. It should be noted that the susceptibility is simply inversely proportional to the average in-plane demagnetizing factor obtained with taking into account the exchange interaction.

By comparing the energies of the vortex state $w(s_0)$ and the uniformly in-plane magnetized state $w_u(h)=2\pi F_1(\beta)-h$, we obtain the critical field

$$h_0(\beta,R)=2a(\beta,R)\left(1-\sqrt{1-\frac{\Delta(\beta,R)}{a(\beta,R)}}\right), \tag{12}$$

where $\Delta(\beta,R)=w_u(0)-w(0)>0$ is the difference between energies when the external field is zero. The condition $\Delta(\beta,R)=0$ gives the critical line $R_c(L)$ and $h_0(\beta,R)=\Delta(\beta,R)$ near the line. The vortex annihilation field can be approximated by using the condition $s_0\approx1$ (vortex center reaches the dot perimeter) in Eq. (11):

$$h_{an}(\beta,R)=2a(\beta,R). \tag{13}$$

Now let us consider the vortex nucleation field. Since the dot radius is large enough, the magnetization reversal will occur via incoherent (nonuniform) nucleation. Here we determine the nucleation field as a maximal field where the originally uniform magnetized (saturated) state becomes un-

stable. However, real nucleation fields differ essentially from theoretical predictions due to defects (pinning centers) within the dots. We assume that a curling magnetization distribution is a nucleation mode wherein a uniformly magnetized state loses stability in the external applied field. The corresponding spin structure is a vortex with its center located outside the disk at a distance of $l_0=R/\sin\varphi_0$ from the disk center, where the angle φ_0 is the intensive variable. This magnetization distribution can be described by the function $f(\zeta)=(i/c)(\zeta-s)$, but with the vortex center displacement $s>1$ ($s=1/\sin\varphi_0$). The case when $\varphi_0=0$ corresponds to the saturated state of a disk with a collinear spin structure (the vortex center position s will go to infinity). We then get for the exchange energy density

$$w_{\rm ex}(\varphi_0)=-\left(\frac{R_0}{R}\right)^2\ln[\cos(\varphi_0)], \tag{14}$$

and the corresponding magnetostatic energy can be obtained from Eq. (7) by the substitution there $s\to 1/\sin(\varphi_0)$ and accounting of uniform dot ($\varphi_0=0$) magnetostatic energy

$$w_m(\varphi_0)=w_m(0)+\frac{2}{\pi}\frac{1}{\sin^2(\varphi_0)}\sum_{\mu>0}F_\mu(\beta)I_\mu^2\left(\frac{1}{\sin(\varphi_0)}\right), \tag{15}$$

and the Zeeman energy density is described by the limit $s\gg 1$ in Eq. (4).

Developing the total magnetic energy of the dot $w_b(\varphi_0)=w_{\rm ex}(\varphi_0)+w_m(\varphi_0)+w_H(\varphi_0)$ into a series on φ_0, followed by a similar expansion on s as in Eq. (9) yields

$$w_b(\varphi_0)=w_b(0)+\frac{1}{2}\varphi_0^2\left[\left(\frac{R_0}{R}\right)^2-\pi F(\beta)+\frac{1}{4}h\right]+O(\varphi_0^4), \tag{16}$$

where $F(\beta)=F_1(\beta)-F_2(\beta)$.

By considering the first and second derivatives of the total magnetic energy with respect to the angle φ_0 we obtain the critical field, below where the uniform magnetic state is unstable. The second derivative at $\varphi_0=0$ $\partial^2 w_b/\partial\varphi_0^2=[(R_0/R)^2-\pi F(\beta)+h/4]$ should be positive. Equation (16) with the condition $\partial^2 w_b/\partial\varphi_0^2=0$ implies that the uniform magnetic state ($\varphi_0=0$) is stable up to the vortex nucleation field:

$$h_n(\beta,R)=4\pi\left[F(\beta)-\frac{1}{\pi}\left(\frac{R_0}{R}\right)^2\right]. \tag{17}$$

Equations (11), (13), and (17) describe analytically the characteristic size-dependent parameters of magnetization reversal in an isolated circular ferromagnetic dot, such as vortex initial susceptibility $\chi(0)$, annihilation $h_{\rm an}$, and nucleation h_n fields within the "rigid" vortex model. Figure 1 shows dependence of the isolated dot critical fields on the value of β. The critical values of R when the functions $h_{\rm an}(\beta,R)$, $h_0(\beta,R)$, and $h_n(\beta,R)$ are equal to zero correspond to the vortex stability radius, the vortex equilibrium radius, and the single-domain state stability radius, respectively.

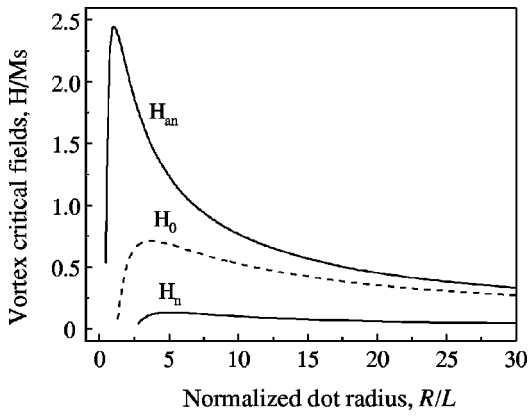

FIG. 1. The dot aspect ratio dependence of the vortex critical fields defined by Eqs. (12), (13), and (17) based on the "rigid" vortex model for $L=20$ nm and $b/L=0.734$.

B. Array of magnetostatically coupled dots

The model described in the preceding section is now extended to the case of typical two-dimensional (2D) dot arrays with a rectangular lattice of nonuniformly magnetized submicron-size disks. We consider the system of identical magnetostatically interacting disks with radius R and dot thickness L. The unit cell sizes are $T_x=2R+d_x$, $T_y=2R+d_y$, where d_x and d_y denote the interdisk spacing along x and y axes, respectively (Fig. 2).

To describe the magnetization reversal in the dot array, we consider the total magnetic energy of the system. The dot exchange energy $W_{\rm ex}$ and the Zeeman energy W_H are single-disk quantities. They thus do not depend on the interdisk spacing d. The magnetostatic energy W_m is influenced by the interdisk interaction, especially for closely packed disk arrays with $\delta=d/R<1$. We assume that all the disks are in the same magnetic state in the external magnetic field.

To calculate W_m, we consider a 2D reciprocal space where the location of the dots can be specified with the reciprocal lattice vector $\mathbf{k}=(k_x,k_y)$. For the rectangular lattice $(k_x,k_y)=2\pi(m/T_x,n/T_y)$, where m and n are integers. We use the general expression for magnetostatic energy density per unit volume of in-plane magnetized patterned film deduced in Ref. 27:

$$W_m=2\pi\sum_k\frac{f(kL)}{k^2}|(\mathbf{k}\cdot\mathbf{M}_k)|^2, \tag{18}$$

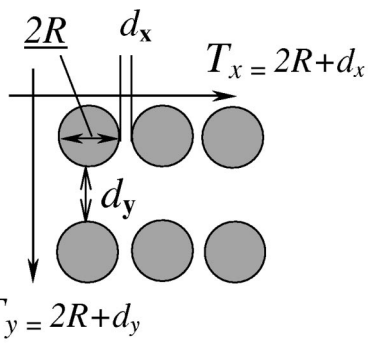

FIG. 2. The geometry of rectangular array of circular ferromagnetic dots used in the present model.

where $f(x)=1-[1-\exp(-x)]/x$, $M_k^\alpha = S^{-1}\int_S d^2\boldsymbol{\rho}\, M^\alpha(\boldsymbol{\rho}) \times \exp(i\mathbf{k}\cdot\boldsymbol{\rho})$, S is the area of a unit cell for the square lattice, and $\boldsymbol{\rho}$ is the radial vector in the x-y plane.

For calculations, we use the magnetization components $\mathbf{M}^\alpha(\rho)$ of the shifted vortex in the ''rigid'' vortex model (Sec. II A). For small s, we obtain the normalized magnetostatic energy density by using similar techniques to Eq. (8), as

$$w_m(s)=w_m(0)+2\pi\Lambda(\beta,\delta,\varphi_H)s^2+O(s^4), \quad \beta=L/R,$$

$$\delta=d_x/R, \tag{19}$$

$$\Lambda(\beta,\delta,\varphi_H)=\frac{4\pi}{T_xT_y}\sum_{\mathbf{k}} f(\beta kR)\frac{J_1^2(kR)}{k^2}\cos^2(\varphi_{\mathbf{k}}-\varphi_H),$$

where $J_1(x)$ is the Bessel function, and φ_k and φ_H are the polar angles for the vectors $\mathbf{k}$ and $\mathbf{H}$.

The function $\Lambda(\beta,\delta,\varphi_H)$ causes uniaxial anisotropy related to the interdisk magnetostatic coupling whereby the easy magnetization axis is directed along the shortest period T_x in the rectangular dot array ($\varphi_H=0$). The vortices are located at the center of each disk in the absence of an external magnetic field. The magnetic charges stored at the small vortex cores and related stray fields do not practically affect the magnetostatic interaction of the disks. This part of the interdisk coupling is negligibly small even for a spacing d close to zero. In an external magnetic field, however, the centers of the vortices are displaced perpendicular to the field direction φ_H, and some magnetic charges appear at the disk circumference, and therein corresponding stray fields originate. This leads to an increase in the intradisk magnetostatic energy followed by the appearance of the interdisk magnetostatic coupling due to nonzero dot dipolar, quadrupolar, and higher-order magnetic moments. The interdisk coupling (being negative) reduces the total magnetostatic energy of the patterned film and therefore favors stabilization of the saturated state. The in-dot magnetostatic energy of the side charges is taken into account by Eqs. (7) and (8) within the ''rigid'' vortex model. Equation (18) includes both the in-dot and interdot magnetostatic energy contributions. $\Lambda(\beta,\delta,\varphi_H)\to F_1(\beta)$ within the limit of isolated dot $\delta\gg 1$ by the substitution

$$\sum_{\mathbf{k}}(\cdots)\to\frac{T_xT_y}{(2\pi)^2}\int d^2\mathbf{k}(\cdots).$$

By minimizing the total magnetic energy, one can obtain the equilibrium shift of the vortex center s as well as the other physical parameters of the dot array. We use decomposition of the energies defined by Eqs. (3), (5), and (19) and rewrite the total energy density in the dimensionless form

$$w(s)=w_{\rm ex}(s)+w_m(s)+w_H(s)$$
$$=w(0)+A(\beta,\delta,R,\varphi_H)s^2-hs+O(s^4),$$

$$A(\beta,\delta,R,\varphi_H)=2\pi\Lambda(\beta,\delta,\varphi_H)-\frac{1}{2}\left(\frac{R_0}{R}\right)^2. \tag{20}$$

This expression for A generalizes Eq. (9) for isolated dots. Since the vortex state is the ground state at $H=0$ for used typical dot parameters ($2R\sim 1\ \mu$m, $L\sim 50$ nm), the coefficient $A(\beta,\delta,R,\varphi_H)>0$. The condition $A(\beta,\delta,R,\varphi_H)=0$ corresponds to the border of vortex stability in the coupled dot array and determine the increase of R_c. Equation (20) immediately leads to the equilibrium displacement s_0 of the vortex center[28] and to the dot average magnetization (dipolar moment) in the magnetic field in the form of Eq. (11), where the parameter $a(\beta,R)$ is replaced by $A(\beta,\delta,R,\varphi_H)$. The dot quadrupolar moment $\hat{Q}\sim s^2$ (Ref. 29) does not contribute to Eq. (20). The initial (anisotropic) magnetic susceptibility of coupled cylindrical dot array applying in-plane field is $\chi_{\rm int}=[2A(\beta,\delta,R,\varphi_H)]^{-1}$.

In the first approximation, the vortex annihilation field $H_{\rm an}$ is determined likely to Eq. (13) by the expression

$$H_{\rm an}(\beta,\delta,R,\varphi_H)=2A(\beta,\delta,R,\varphi_H)M_s. \tag{21}$$

The in-dot magnetostatic interaction gives positive and the in-dot exchange interaction and interdot magnetostatic coupling (through induced stray fields) give negative contributions to the dot annihilation field. For $R=0.1$–$1\ \mu$m, the vortex shift is mainly determined by competition between magnetostatic and Zeeman energies. Both the susceptibility and $H_{\rm an}$ reveal uniaxial anisotropy in the rectangular dot array with easy axis $\varphi_H=0$ (Ox), parallel to the close-packed direction in the rectangular dot lattice.

To estimate the vortex nucleation field in the dot array we should consider the stability of magnetized rectangular dot array in an external magnetic field. Let magnetic field is parallel to one of the dot lattice [10] or [01] direction. We need only recalculation of the magnetostatic energy for the dot array given for isolated dot by Eq. (15). The magnetization distribution $\mathbf{m}(\rho)$ in each dot is given by the function $f(\zeta)=(i/c)(\zeta-s)$ where $s\gg 1$. Detailed calculation on the basis of Eq. (18) leads to the substitution of the function $F(\beta)$ in Eqs. (16) and (17) to the function

$$F(\beta,\delta,\varphi_H)=-\frac{8\pi}{T_xT_y}\sum_{\mathbf{k}} f(\beta kR)\frac{\cos^2(\varphi_{\mathbf{k}}-\varphi_H)}{k^2}$$
$$\times[C_1(kR)\cos 2(\varphi_{\mathbf{k}}-\varphi_H)+C_2(kR)], \tag{22}$$

where the coefficients are $C_1(x)=3J_1(x)J_3(x)-J_2^2(x)$ and $C_2(x)=-J_1(x)J_3(x)-J_0(x)J_2(x)$. Then, the nucleation field h_n for the magnetostatically coupled rectangular dot array has the following form:

$$h_n(\beta,\delta,R,\varphi_H)=4\pi\left[F(\beta,\delta,\varphi_H)-\frac{1}{\pi}\left(\frac{R_0}{R}\right)^2\right]. \tag{23}$$

This field decreases rapidly when decreasing the relative interdot distance δ. The nucleation field h_n exhibits a more complex anisotropy than the uniaxial one. This is due to the presence of a considerable contribution of high-order intradot magnetic multipolar moments (quadrupolar, Q, in par-

ticular) to the interdot magnetostatic coupling. This effect is essential for close-packed rectangular dot arrays with $d/R < 0.5$.[29]

III. MICROMAGNETIC CALCULATIONS

The magnetic behaviors of individual and interacting disks were separately examined using Landau-Lifshitz-Gilbert (LLG) micromagnetic solver.[30] The solver has been successfully used for calculating hysteresis loops and domain structures in small ferromagnetic particles.[31] The computational material parameters are typically for Permalloy the saturation magnetization $M_s = 8.0 \times 10^5$ A/m and the exchange stiffness constant $C = 1.3 \times 10^{-11}$ J/m. The magnetocrystalline anisotropy is neglected. A systematical study on the effect of discretization and of the element size on calculated hysteresis loops was performed prior to the main calculations. Comparison between 2D and 3D discretization schemes shows that the obtained results are almost identical for the flat disk with $L < R$. The unit element size is 4 nm $\times 4$ nm $\times L$. Decreasing the element size does not influence the numerical results, even for the smallest disks calculated. Note that the unit element size is much smaller than the exchange length of the system ($\sim$14 nm) so that the spin distribution in the vortex core can be described correctly. The evolution of the spin structure, the average magnetization components, and the dot energy terms were calculated as a function of an in-plane applied magnetic field. The initial susceptibility $\chi(0)$ was determined as a slope of the linear part of the magnetization curve at zero field. The critical fields where the spin structure transforms from the vortex to the single domain state and vice versa were defined as annihilation H_{an} and nucleation H_n fields, respectively.

The effect of interdot magnetostatic interaction on magnetization reversal was elucidated for the dots placed in a finite chain. The susceptibility $\chi(0)$ and critical fields H_n and H_{an} of the central dot in the chain were used for comparison with the analytical model. The chain configuration corresponds to the limit of the dot array with a rectangular lattice where the interdisk distance along one direction is kept much larger than the dot radius. We thus neglect the magnetostatic interaction between the individual chains in the array. In the analytical model, the magnetostatic energy described by Eq. (18) includes the effect of all the surrounding disks. Therefore the susceptibility, nucleation, and annihilation fields given by Eqs. (21) and (23) correspond to the infinitely large dot array. By comparing the micromagnetic hysteresis loops for the chains with different number of dots from 3 to 13 and small interdot distance, we conclude that at least seven elements have to be considered in the calculation in order to correctly treat the effects of long-range magnetostatic interaction. The switching behavior of the central dot does not vary with increase of the number of elements and can be considered as a good approximation to the infinite chain. Detailed discussion of analytical calculations for smaller number of the elements will be reported elsewhere. The disk thickness L is chosen to be 40 or 60 nm and the interdot distance d is varied from 400 nm down to 30 nm. The external magnetic field was applied along the chain. The isolated dot diameter is varied from 0.1 to 0.6 μm and disk thickness from 10 to 60 nm. The micromagnetic calculation is time consuming, especially for the chain of the dots: therefore, the dot diameter in this case was fixed to be 0.4 μm only.

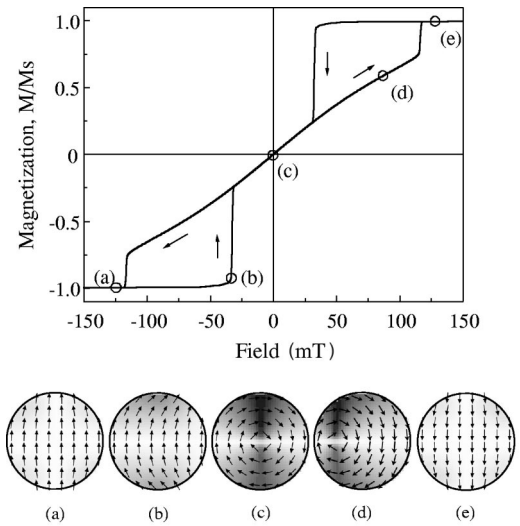

FIG. 3. The typical hysteresis loop and magnetization reversal process due to the vortex nucleation, displacement, and annihilation as calculated with micromagnetic solver for an isolated dot with $R = 0.1$ μm and $L = 30$ nm.

IV. RESULTS AND DISCUSSION

Figure 3 shows a typical hysteresis loop and the field evolution of the spin structure, calculated with the LLG solver for the circular dots, 0.2 μm in diameter and 30 nm in thickness. When the magnetic field is decreased from saturation [Fig. 3(a)], a magnetic vortex nucleates in the nucleation field H_n [Fig. 3(b)] accompanied by an abrupt decrease in the average dot magnetization. This results in a gain in the magnetostatic energy. The center of the vortex stays at the center of the dot [Fig. 3(c)] at $H = 0$. The reversible part of the loop corresponds to the vortex core movement perpendicular to the applied field [Fig. 3(d)]. When the magnetic field reaches the annihilation field H_{an}, the vortex vanishes completely. This process stabilizes the single-domain state in the dot [Fig. 3(e)]. The values of H_n, H_{an}, and the slope of the linear part of the hysteresis loop are strongly size dependent. The magnetization distribution in Figs. 3(a) and 3(e) is slightly nonuniform, especially near the dot edges (''*leaf*'' state[8]), to reduce side surface magnetostatic energy. But we will neglect these deviations.

Figure 4 compares the initial susceptibility $\chi(0)$ of the vortex state determined using the micromagnetic calculations (open markers) and analytical results given by Eq. (11) (solid lines) as a function of the dot aspect ratio $\beta = L/R$. The dot radius R is well above of R_c, and the exchange contribution is negligible. The analytical model is in excellent agreement with micromagnetic data for a variety of β. These results coincide well with the experimental data obtained for 60-nm-thick submicron circular Permalloy dots.[28] The value of $\chi(0)$ increases with decreasing β; e.g., the vortex core has higher

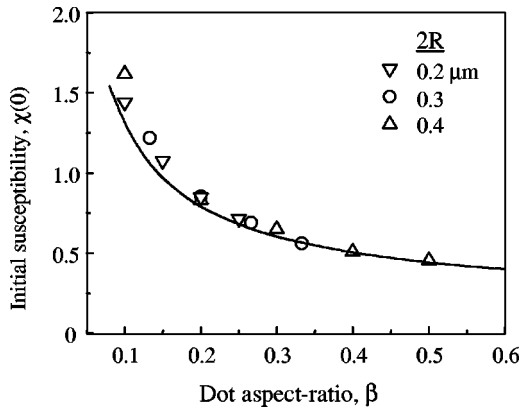

FIG. 4. The initial susceptibility (solid line) calculated using Eq. (7) together with micromagnetic data (open markers) as obtained for isolated circular dots with variable diameter $2R$ and thickness L.

mobility for the dots with larger diameter or smaller thickness. Note that the susceptibility of the single vortex has the smallest value for intermediate $\beta \sim 0.5$ and increases sharply for the dot with diameter close to the dot's instability region due to expected transition of the vortex state to the in-plane magnetized single domain state. The values of $R_c(L)$ determined from the equation $a(\beta,R)=0$ by Usov and Peschany[24] are much smaller than those calculated in the Ref. 25 by using two-vortex model more correct values.

Figure 5 summarizes the data for the vortex nucleation and annihilation fields for an isolated circular dot with variable R and L. The solid lines are plotted using Eqs. (13) and (17), and the symbols represent micromagnetic calculations. The analytical results agree well with the micromagnetic LLG calculations except for the H_n values for large R, where other nucleation modes can be realized, indicating that the vortex nucleation occurs in the dot with a relatively small diameter, and quite a strong field required to uniformly magnetize the dots. Therefore, the magnetization reversal due to the vortex nucleation and annihilation is not desirable for MRAM memories with in-plane magnetized cells.[20] As the dot diameter increases, both the nucleation and annihilation

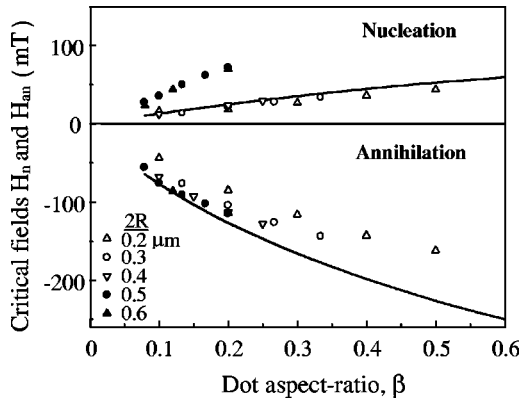

FIG. 5. The vortex nucleation and annihilation fields (solid lines) calculated using Eqs. (13) and (17) together with micromagnetic data (open and solid symbols) as obtained for isolated circular dots with variable radius R and thickness L.

fields decrease. The vortex magnetic state is the ground state of the system, and the nucleation field is always smaller than the annihilation field.

As can be expected from Eqs. (11), (13), and (17), the initial susceptibility, the vortex, nucleation and annihilation fields are predetermined by saturation magnetization M_s and the dot aspect ratio β. As far as R is much larger than the exchange length, the magnetostatic energy dominates, and the absolute values of dot radius R and the dot height L are not important. This means that the model yields identical results for H_n, $\chi(0)$, and $H_{\rm an}$ for the dots with different values of R and L, but the same aspect ratio β. The solid lines in Figs. 4 and 5 can be viewed within the framework of ''rigid'' vortex model as universal curves of the characteristic parameters of magnetization reversal process. As we mentioned above, the proposed model for the shifted vortex magnetization distribution is valid only for weak magnetic fields when the vortex core displacement s is small. The values of $H_{\rm an}$ were determined by extrapolating the linear part of $M(H)$ up to saturation M_s. Therefore, the analytical results of $\chi(0)$, equivalent to a reversible vortex displacement in small fields, are in full agreement with micromagnetic results for all the dots studied here. There are some evident disagreements with numerical results for the H_n and $H_{\rm an}$ as discussed below.

The analytical equation (13) for the annihilation field closely follows the micromagnetic data for the dots with smaller aspect ratio β and larger dot radius R, but it fails when $R<0.1\,\mu$m and $\beta>0.5$. For the fixed value of β, the discrepancy tends to increase with decreasing the dot radius R. Within the ''rigid'' vortex model we are able to use the higher-order terms in the expansion on the parameter s for the Eqs. (2), (4), and (7). More detailed analyses show that the model overestimates the magnetostatic energy for $s \to 1$ and, thus, the vortex annihilation field, especially for small R. When the vortex core approaches the circumference of dots ($s \leqslant 1$), the elliptically deformed vortex shape should be taken into account. This will effectively reduce the magnetostatic energy due to the decrease in surface charge along the dot perimeter. A possible way to improve the model for proper values of $H_{\rm an}$ is to introduce the field-dependent vortex core radius.[26] However, this approach does not yield the vortex stability radius and correct initial susceptibility. Then all the magnetic energy terms will be modified. The influence of the vortex deformation becomes crucially important for a dot with a very small diameter (near the critical radius R_c of the vortex stability), since the vortex core occupies almost all the dot volume.

All the calculated vortex nucleation fields can be classified into two groups in accordance with the dot radius as is clearly seen in Fig. 5, where the nucleation field H_n is plotted as a function of the aspect ratio β. The micromagnetic data for the first group (open symbols) correspond to the data for dots with $R \leqslant 0.2\,\mu$m, in excellent agreement with the analytical results given by Eq. (17) (solid line). The value of H_n in the second group (solid symbols) for dots with $R > 0.2\,\mu$m has a larger nucleation field than the analytical results. The discrepancy is more pronounced for larger β. In our simple assumption, the magnetization reversal was initi-

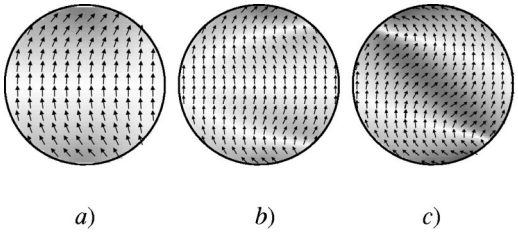

FIG. 6. The spin instabilities modes obtained with micromagnetic calculations for the circular dots with the $R=0.1$ (a), 0.2 (b), and 0.25 μm (c) and fixed $L=30$ nm.

ated by the ''*C-shape*'' nucleation mode as shown in Fig. 6(a). This mode is described quite well by the ''rigid'' vortex model. Micromagnetic calculations show that there are other spin structures with close energy just before nucleation for small dots. Figure 6 shows the metastable spin structures calculated for the dots with $L=30$ nm and $R=0.1$, 0.2, and 0.3 μm. With increasing dot diameter, the spin structure gradually transforms from ''*C-shape*'' [Fig. 6(a)] to ''*buckling*'' [Fig. 6(b)] and then to ''*S-shape*'' [Fig. 6(c)] configurations. The dot aspect ratio β seems to have no effect on the in-plane magnetic states. Interesting to note is that the configurations in Figs. 6(a) and 6(b) end up with a single vortex. On the other hand, two vortices are nucleated on the dot side surface at much higher field for the nucleation mode shown in Fig. 6(c). The different nucleation modes appear to be responsible for the discrepancy between the analytical and the micromagnetic results. The magnetization reversal accompanied by the nucleation of two vortices was studied experimentally in submicron disks[19] and with micromagnetics in ellipsoidal permalloy dots.[32] The validity of the analytical solution, likely given by Eq. (17), can be extended for the dots with $R>0.2\,\mu$m if one takes a more complicated magnetization distribution into consideration for the energy description. The theoretical expression of the size-dependent transition between different nucleation modes still remains to be deduced.

Figure 7 shows a typical micromagnetic hysteresis loop for the chain of seven identical circular dots with radius $R=0.2\,\mu$m, thickness $L=60$ nm, and separating distance $d=50$ nm. As follows from previously described micromagnetic data, the magnetization reversal process in a small dot is always accompanied by only one sharp jump in magnetization, corresponding to an irreversible transition from a collinear to a vortex spin structure. The demagnetization curve for the chain exhibits a stepwise decrease, because the vortices nucleate at different fields for the different dots. The field evolution of the spin structure in the chain is given in Fig. 8. In high magnetic fields, all spins are aligned along the field [Fig. 8(a)]. With decreasing field the vortex nucleation is first initiated in two dots located at the ends of the chain [Fig. 8(b)]. These dots are neighbor free in one side, and they are consequently subjected to an effective magnetic field, which is smaller than the one for other dots inside of the chain. After the nucleation, the vortex core stays quite far from the dot center [Fig. 8(c)], according to the balance between the magnetostatic and Zeeman energies. The magnetic charges induced on the side surface result in a non-negligible stray magnetic field around the dot. Therefore the ending dots with magnetic vortices are still magnetostatically coupled with other elements of the chain. This coupling decreases drastically with decreasing field because of the vortex core displacement toward the dot centers. The contribution of the out-of-plane dot magnetization component can be ignored here, since the dot radius is much larger then the radius of the vortex core. As a result, the magnetization reversal process is progressively initiated in the neighboring dots toward the center of the chain [Figs. 8(d) and 8(e)]. In remanence (zero applied field) the dots are in the vortex magnetic states. The centers of the vortices are at the center of the dots. Therefore, the magnetic ''charges'' are practically absent and magnetostatic interaction between the individual the dots is negligibly small, even though for distances d close to zero. However, once the external magnetic field is applied to the system, the centers of vortices are shifted and some magnetic ''charges'' arise on the dots boundaries. This leads to increasing the self-magnetostatic energy of the dots described by Eq. (19) and appearing the interdot magnetostatic interaction.

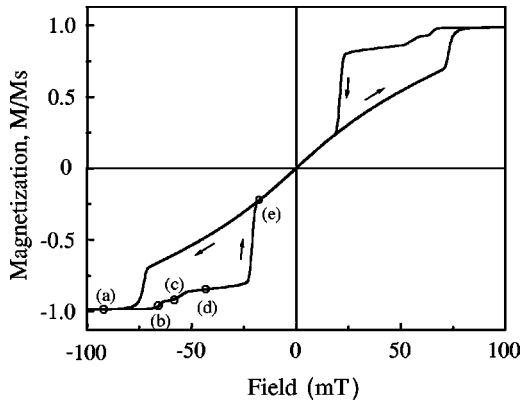

FIG. 7. The descending part of the micromagnetic hysteresis loops for the chain of seven dots with $R=0.2\,\mu$m, $L=60$ nm, and $d=50$ nm.

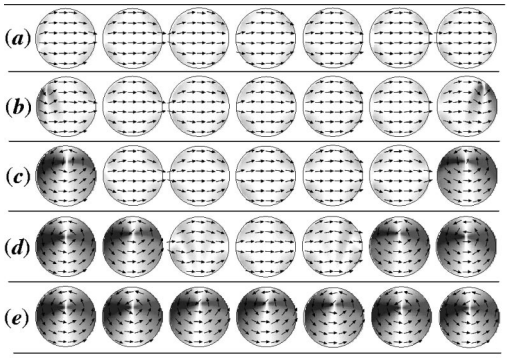

FIG. 8. The evolution of the spin structure in the chain of circular dots for different magnetic fields marked by the open circles in Fig. 7.

Figure 9 compares the initial susceptibility $\chi(0)$ obtained from micromagnetic and analytical calculations for a magnetic field applied along the shortest unit cell period ($\varphi_H=0$). We have reasonably good agreement between the cal-

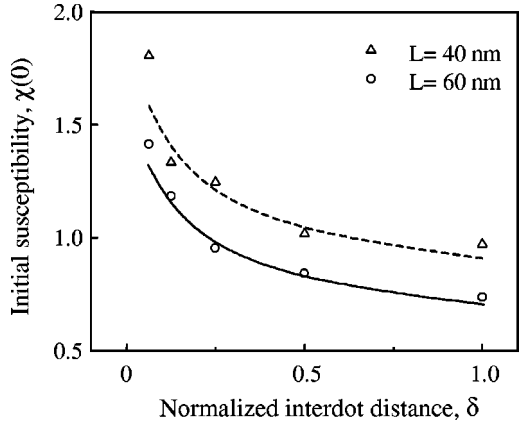

FIG. 9. The initial susceptibility (dashed line, $L=60$ nm; solid line, $L=40$ nm) calculated using Eq. (20) together with corresponding micromagnetic data (open markers) for the chain of the dots vs. the normalized interdot distance $\delta=d/R$.

culations and experiments except for the limit $d/R>0$. This means that the ''rigid'' vortex model is applicable to account for the interdot magnetostatic coupling. The vortex nucleation and annihilation fields $H_n(d/R)$ and $H_{\rm an}(d/R)$ are normalized to the corresponding values in isolated dots ($d/R \gg 1$) with the same geometry and are shown in Figs. 10 and 11. Both the analytical model and the micromagnetic data clearly show that the magnetostatic interdot plays an important role in the magnetization reversal in arrays with $\delta = d/R<0.5$, leading to a decrease in H_n, $H_{\rm an}$, and an increase in $\chi(0)$.

We had good quantitative agreement between the interdot spacing dependences of $H_{\rm an}$ obtained from both analytical and numerical calculations as seen in Fig. 10. This implies that the vortices annihilate almost collectively in the dot array and allow us to regard all the dots as identical. But the physical picture for the nucleation field is more complex. Equation (23) predicts more rapid decrease of H_n than the micromagnetic result when decreasing the interdot spacing d (Fig. 11). According to the micromagnetic calculation in Fig.

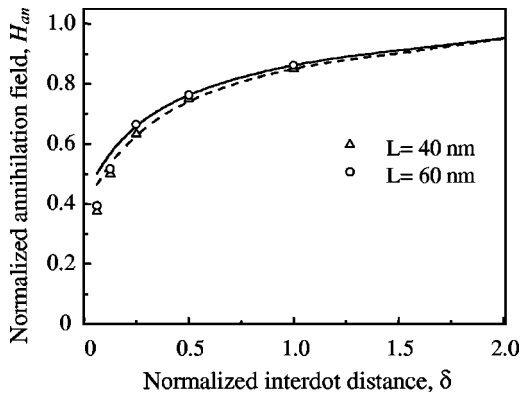

FIG. 10. The normalized annihilation fields $H_{\rm an}(d/R)/H_{\rm an}$ (isolated dot) (line, $L=40$ nm; solid line, $L=60$ nm) calculated using Eq. (21) for the rectangular dot array together with corresponding micromagnetic data (open markers) for chain of the dots vs the normalized interdot distance $\delta=d/R$.

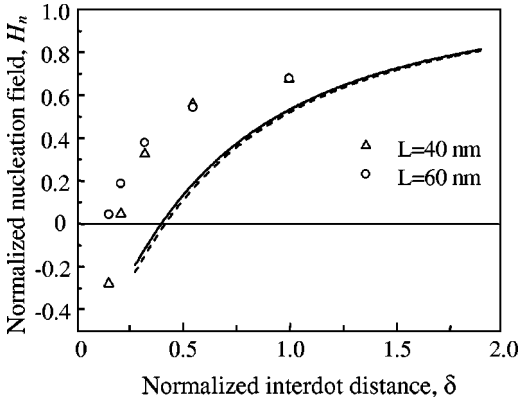

FIG. 11. The normalized nucleation fields $H_n(d/R)/H_n$ (isolated dot) (dashed line, $L=60$ nm; solid line, $L=40$ nm) calculated using Eq. (23) plotted with corresponded micromagnetic data for the chain of the dots vs the normalized interdot distance $\delta=d/R$.

8, the nucleation initiates at the edges of the chain to propagate toward the center, indicating that the nucleation process is not uniform. The mean field approximation based on Eqs. (18) and (22) shows that the strength of the dipolar coupling is proportional to the magnetization averaged over the chain. This approximation now fails to explain qualitatively the nonuniform nucleation process. In the approximation, all the dots are assumed to have an identical magnetic configuration with the same dot magnetization. However, the magnetization of the dot with nonuniform nucleation is smaller than the average. This reduces the interdot coupling and results in the higher values of the nucleation field $H_n(d/R)$ compared to the mean-field approximation. A detailed discussion of the nucleation in coupled dots is out of the scope of this paper and will be discussed elsewhere. Note that the both $H_n(d/R)$ and $H_{\rm an}(d/R)$ follow their universal lines when plotted into normalized coordinates. Therefore, δ is considered to be a key parameter to compare the effect of magnetostatic interaction on magnetization reversal in submicron dot arrays with different L and R. For the dots with smallest δ the chain is stabilized in the single-domain remanent state and nucleation field becomes negative. The similar effect was observed by Cowburn *et al.*[33] In their work, the transition from superparamagnetic to ferromagnetic ordering in Permalloy dot arrays ($R=30$ nm, $L=10-20$ nm) induced by interdot interaction was reported. The rectangular dot arrays were investigated for cobalt,[6,7] Permalloy,[11,12] and iron dots.[5] However the effect of anisotropic interdot magnetostatic coupling was suppressed by the strong shape and magnetocrystalline anisotropies.

V. CONCLUSIONS

The ''rigid'' vortex model was used to describe analytically the characteristic parameters of the magnetization reversal in individual circular dots and magnetostatically coupled rectangular arrays with ''vortex'' remanent state by using only the geometry of the dot L and R, interdot distance d, and the saturation magnetization M_s. The proposed analytical description is in good qualitative and, sometimes,

quantitative agreement with micromagnetic data for the most important practical case of the flat submicron dot arrays with $R \sim 0.1-0.3\ \mu$m and $\beta = L/R < 0.2$. The nucleation and annihilation fields decrease, whereas the initial susceptibility increases with decreasing the dot aspect ratio β. The effect of interdot magnetostatic interaction is rather small and therefore can be ignored for the dots in ''vortex'' state, in zero magnetic field, and for the dot arrays with $\delta = d/R > 1$. On the other hand, the interdot interaction has a strong destabilizing effect on the vortex spin state in dot arrays with small interdot distance, leading to a significant decrease of both the vortex critical fields H_n, H_{an}, and an increase in the initial susceptibility $\chi(0)$. The origin of this coupling is the appearance of dot side surface charges induced by an external field.

ACKNOWLEDGMENTS

This work was supported in part by Korea Institute for Advanced Study, RFTF of the Japan Society for the Promotion of Science, and the Grant-in-Aid for Scientific Research from the Ministry of Education, Science, and Culture in Japan. Valuable discussions with Dr. Olivier Fruchart are acknowledged.

*Author to whom correspondence should be addressed. Present address: Argonne National Laboratory, Materials Science Division, Bldg. 223, IL 640439. Electronic address: novosad@anl.gov

[1] S. Tehrani, E. Chen, M. Durlam, M. DeHerrera, J. M. Slaughter, J. Shi, and G. Kerszykowski, J. Appl. Phys. **85**, 5822 (1999).
[2] S. Y. Chou, Proc. IEEE **85**, 652 (1997).
[3] C. A. Ross, H. I. Smith, T. Savas, M. Schattenburg, M. Farhoud, M. Hwang, M. Walsh, M. C. Abraham, and R. J. Ram, J. Vac. Sci. Technol. B **17**, 3168 (1999).
[4] R. P. Cowburn, D. K. Koltsov, A. O. Adeyeye, and M. E. Welland, J. Appl. Phys. **87**, 7082 (2000).
[5] A. Aharoni, *Introduction to the Theory of Ferromagnetism* (Oxford University Press, New York, 2001).
[6] M. Hehn, K. Ounadjela, R. Ferré, W. Gramge, and F. Rousseaux, Appl. Phys. Lett. **71**, 2833 (1997).
[7] Y. Otani, T. Kohda, V. Novosad, K. Fukamichi, S. Yuasa, and T. Katayama, J. Appl. Phys. **87**, 5621 (2000).
[8] R. P. Cowburn, J. Phys. D **33**, R1 (2000).
[9] M. Schneider and H. Hoffman, J. Appl. Phys. **86**, 4539 (1999).
[10] A. Fennandez and C. J. Cerjan, J. Appl. Phys. **87**, 1395 (2000).
[11] M. Grimsditch, Y. Jaccard, and I. K. Schuller, Phys. Rev. B **58**, 11 539 (1998).
[12] K. Runge, Y. Nozaki, Y. Otani, H. Miyajima, B. Pannetier, T. Matsuda, and A. Tonomura, J. Appl. Phys. **79**, 5075 (1996).
[13] D. K. Koltsov, R. P. Cowburn, and M. E. Welland, J. Appl. Phys. **88**, 5315 (2000).
[14] A. Aharoni, J. Appl. Phys. **68**, 2892 (1990).
[15] J. Raabe, R. Pulwey, R. Sattler, T. Schweinbock, J. Zweck, and D. Weiss, J. Appl. Phys. **88**, 4437 (2000).
[16] R. P. Cowburn, D. K. Koltsov, A. O. Adeyeye, M. E. Welland, and D. M. Tricker, Phys. Rev. Lett. **83**, 1042 (1999).
[17] V. Novosad, K. Yu. Guslienko, Y. Otani, H. Shima, K. Fukamichi, N. Kikuchi, O. Kitakami, and Y. Shimada, IEEE Trans. Magn. **EMG-37**, 2088 (2001).
[18] T. Shinjo, T. Okuno, R. Hassdorf, K. Shigeto, and T. Ono, Science **289**, 5481 (2000).
[19] T. Pokhil, D. A. Song, and J. Nowak, J. Appl. Phys. **87**, 6319 (2000).
[20] J. Shi, S. Tehrani, and M. R. Scheinfein, Appl. Phys. Lett. **18**, 2588 (2000).
[21] J.-G. Zhu, Y. Zheng, and G. Prinz, J. Appl. Phys. **87**, 6668 (2000).
[22] N. Kikuchi, S. Okamoto, O. Kitakami, Y. Shimada, S. G. Kim, Y. Otani, and K. Fukamichi, IEEE Trans. Magn. **EMG-37**, 2082 (2001).
[23] N. A. Usov and S. E. Peschany, J. Magn. Magn. Mater. **118**, L290 (1993).
[24] N. A. Usov and S. E. Peschany, Fiz. Met. Metalloved. **12**, 13 (1994).
[25] K. L. Metlov and K. Yu. Guslienko (unpublished).
[26] K. Yu. Guslienko and K. L. Metlov, Phys. Rev. B **63**, 100403 (2001).
[27] K. Yu. Guslienko, Appl. Phys. Lett. **75**, 394 (1999).
[28] K. Yu. Guslienko, V. Novosad, Y. Otani, H. Shima, and K. Fukamichi, Appl. Phys. Lett. **78**, 3848 (2001).
[29] K. Yu. Guslienko, Phys. Lett. A **278**, 293 (2001).
[30] M. J. Donahue and D. G. Porter (unpublished).
[31] http://math.nist.gov/oommf/bibliography.html
[32] N. A. Usov, C.-R. Chang, and Z.-H. Wei, J. Appl. Phys. **89**, 7591 (2001).
[33] R. P. Cowburn, A. O. Adeyeye, and M. E. Welland, New J. Phys. **1**, 16 (1999).